Cancer Chemother Pharmacol (2008) 61:791–802
DOI 10.1007/s00280-007-0536-2

ORIGINAL ARTICLE

Proteomic analysis of liver cancer cells treated with suberonylanilide hydroxamic acid

Aiping Tong · Haiyuan Zhang · Zhengyu Li · Lantu Gou · Zhi Wang · Haiyan Wei · Minghai Tang · Shufang Liang · Lijuan Chen · Canhua Huang · Yuquan Wei

Received: 10 March 2007 / Accepted: 25 May 2007 / Published online: 26 June 2007

Abstract
Purpose Suberonylanilide hydroxamic acid (SAHA) is an orally administered histone deacetylase inhibitor (HDACI) that has shown significant antitumor activity in a variety of tumor cells. To evaluate if SAHA has an activity against liver cancer, and with an aim to identify the altered cellular factors upon SAHA treatment, human HepG2 cancer cell line was used as a model, and proteomic approach was utilized to elucidate the molecular mechanisms underlying SAHA's antitumor activity.
Methods Cell growth inhibition was measured by MTT method, and apoptosis was detected by means of flow cytometry analysis and TUNEL assay. Protein expression profiles were analyzed by 2-DE coupled with MALDI-Q-TOF MS/MS analysis.
Results A total of 55 differentially expressed proteins were visualized by 2-DE and Coomassie Brilliant Blue (CBB) staining. Of these, 34 proteins were identified via MS/MS analysis. Among the identified proteins, six proteins also displayed significant expression changes at earlier time points upon SAHA treatment, and such alterations were further confirmed by semi-quantitative RT-PCR. Together, at both the mRNA and protein levels, SAHA suppressed the expression of reticulocalbin 1 precursor (RCN1), annexin A3 (ANXA3) and heat shock 27 kDa protein 1 (HSP27), while increasing the expression of aldose reductase (AR), triosephosphate isomerase 1 (TPI) and manganese superoxide dismutase (SOD2).
Conclusion SAHA remarkably inhibited proliferation of HepG2 cancer cells, and induced apoptosis in vitro. Using proteomics approaches, a variety of differentially expressed proteins were identified in HepG2 cancer cells before and after treatment with SAHA. This study will enable a better understanding of the molecular mechanisms underlying SAHA-mediated antitumor effects at the protein level.

Keywords Proteomics · 2-DE · HDACIs · Suberonylanilide hydroxamic acid · Hepatocellular carcinoma · HepG2

Abbreviations

SAHA	Suberonylanilide hydroxamic acid
HADC	Histone deacetylase
HADCIs	Histone deacetylase inhibitors
2-DE	2-Dimensional polyacrylamide gel electrophoresis
HCC	Hepatocellular carcinoma
RCN1	Reticulocalbin 1
ANXA3	Annexin A3
HSP27	Heat shock 27 kDa protein 1
AR	Aldose reductase
TPI	Triosephosphate isomerase 1
SOD2	Manganese superoxide dismutase

A. Tong · Z. Li · L. Gou · H. Wei · M. Tang · S. Liang · L. Chen · C. Huang (✉) · Y. Wei (✉)
The State Key Laboratory of Biotherapy, West China Hospital, and College of Life Science, Sichuan University, Chengdu 610041, People's Republic of China
e-mail: hcanhua@hotmail.com

Y. Wei (✉)
e-mail: yuquawei@vip.sina.com

H. Zhang
The School of Medicine, Yangtze University, Shashi, Hubei Province 434000, People's Republic of China

Z. Wang
Department of Oral Mucosal Diseases, West China Stomatological Hospital, Sichuan University, Chengdu 610041, People's Republic of China

Introduction

Histone deacetylase inhibitors (HDACIs) induce hyperacetylation of core histones, modulate chromatin structure and affect gene expression [1, 2]. HDACIs have been reported to induce cell growth arrest, differentiation, and/or promote apoptotic cell death in a variety of tumor cells in vitro as well as in vivo [3, 4]. Suberoylanilide hydroxamic acid (SAHA), the prototype of synthetic hydroxamic acid-based hybrid polar HDACIs, binds directly to the histone deacetylase catalytic site, inhibits its enzymatic activity [5] and exerts antiproliferative and/or proapoptotic effects restricted to transformed cells [6]. It can be administered orally and has been approved by the FDA for the treatment of cutaneous T-cell lymphoma (CTCL).

SAHA has been shown to induce cell growth inhibition through up-regulation of $p21^{WAF1}$ [7], as well as promote apoptosis through mitochondrial mediated processes involving cleavage of Bid and production of reactive oxygen species (ROS) [8], induction of caspase activation [9] and regulation of NF-κB [10] and thioredoxin pathway [11]. Even though a panel of genes modulated by SAHA have been identified, the complex mechanisms underlying its antiproliferative effects remain elusive.

Hepatocellular carcinoma (HCC) is one of the most common malignancies in the world with an estimated half a million deaths annually, and its incidence is on the rise in the USA, Europe and Asia [12, 13]. HCC is highly resistant to chemotherapy, and most current therapeutic strategies against HCC are unsatisfactory [14]. Studies have shown that trichostatin A (TSA) can suppress cell proliferation, induce cell-cycle arrest/apoptosis and promote differentiation of hepatocytes in human hepatoma cells [15, 16]. Armeanu et al. [17] found that HDACIs VPA and ITF2357 can preferentially induce cell death in HCC-derived cell lines, whilst showing little or no toxicity against primary human hepatocytes.

2-DE based proteomics provided us a useful tool to rapidly profile altered cellular factors in response to drug treatment [18–20]. In this study, a hepatoma cell line HepG2 was used as a model, and 2DE-MS strategy was utilized to unravel the changed proteins following SAHA treatment in order to better understand the molecular mechanism underlying its anti-tumor activity. To determine the generality of the changed proteins, a comparison of SAHA-induced protein alterations was performed between HepG2 and Jurkat lymphoma cell line, which was highly sensitive to SAHA [21].

Materials and methods

Cell culture and treatment

HepG2 and Jurkat cell lines were purchased from ATCC (Rockville, MD, USA). Cells were maintained in Dulbecco's modied Eagle's medium (DMEM, Gibco, USA) containing 10% fetal calf serum (Hyclone, USA), penicillin (10^7 U/l) and streptomycin (10 mg/l) at 37°C in an atmosphere containing 5% CO_2. SAHA was purchased from (Alexis, San Diego, CA). A 10 mM solution of SAHA was prepared in DMSO, and stored as small aliquots at −20°C. Cells were seeded at a density of 0.5×10^6 per plate (10 cm^2). When the cells reached 80% confluency, the medium was replaced by a fresh culture medium containing SAHA. Control cells were cultured in a medium containing equal amount of DMSO instead of SAHA. For 2-DE analysis, HepG2 cells were treated with 5 μM SAHA for 12, 24 or 48 h, respectively. Jurkat cells were treated with 2.5 μM SAHA for 48 h. Cells were washed twice by centrifugation in PBS and transferred to sterile plastic tubes for storage at −80°C until use.

Cell proliferation assay

Cells were plated in 96-well cell culture plates (1.5×10^3 cells/well) and treated with SAHA for 48 h at the indicated concentrations, and then 20 μl of MTT (5 mg/ml) was added to each well. After 4 h incubation, the medium was removed from the wells and 150 μl of DMSO was added. The absorbance was measured at 570 nm in an enzyme-linked immunosorbent assay reader. Results were expressed as the fractional survival of treated cells normalized to control cells (control cells were considered to be 100% survival). The data represent three independent experiments performed in triplicate. The results were tested for statistical significance by ANOVA. A P value less than 0.05 was considered as significant.

Flow cytometry

Flow cytometry analysis was performed to measure apoptosis using propidium iodide (PI) staining. After incubation with 5 μM SAHA for 24 or 48 h, the cells were washed with PBS twice and harvested by trypsinization. The cells were washed again with PBS and fixed by incubation in 50% ice-cold ethanol/PBS for 30 min on ice. After washing with PBS once more, the cells were then re-suspended and incubated in PI solution (70 μM propidium iodide, 38 mM sodium citrate and 20 μg/ml RNase A) for 30 min at 37°C. Flow cytometry analyses were performed on a FACScan flow cytometry system (Becton Dickinson, San Jose, CA). Data were analyzed using winMDIv2.8 software. Three independent experiments were carried out. Results were tested for statistical significance by Student's t test. Significance was defined as $P < 0.05$.

TUNEL assay

TUNEL assay was performed using the DeadEnd™ Fluorometric TUNEL system (Promega Inc., Madison, WIS).

Cells were grown on chamber slides overnight and treated with 5 μM SAHA for 48 h. Prior to TUNEL assay, the cells were washed with PBS twice and fixed by 4% methanol-free formaldehyde solution in PBS for 25 min at 4°C, followed by permeabilizing with 0.2% Triton X-100 in PBS for 5 min at room temperature. Staining was done according to the manufacturer's instructions. Fluorescence was visualized with Olympus BX60 microscope (Olympus Optical Co., Hamburg, Germany). Three independent experiments were carried out. Results were tested for statistical significance (Student's *t* test, $P < 0.05$).

2-DE and image analysis

About 3×10^7 cells were lyzed in 1 ml lysis buffer (7 M urea, 2 M thiourea, 4% CHAPS, 100 mM DTT, 2% pH 3–10 ampholyte, BioRad, USA) containing protease inhibitor cocktail 8340 (Sigma, St Louis, MO, USA). Samples were then kept on ice and sonicated in six cycles of 10 s, each consisting of 5 s sonication followed by a 10 s break, and finally held for 30 min on ice with occasional vortex mixing. After centrifugation at 14,000 rpm for 1 h at 4°C, proteins were precipitated with cold acetone at −20°C for 1 h and then dissolved with rehydration buffer (8 M urea, 2 M thiourea, 4% CHAPS, 100 mM DTT, and 2% ampholyte). Protein concentrations were determined using the DC protein assay kit (Bio-Rad). Individual sample concentrations were adjusted by dilution in the same rehydration buffer. Samples were either applied immediately to Isoelectric Focusing (IEF) or stored at −80°C in aliquots prior to analysis. Protein samples (300 (μl) were applied to IPG (immobilized pH gradient) strip (17 cm, pH 3–10, NL, Bio-Rad) using a passive rehydration method. After 12–16 h of rehydration, the strips were transferred to an IEF Cell (Bio-Rad). IEF was performed as follows: 250 V for 30 min, linear; 1,000 V for 1 h, rapid; linear ramping to 10,000 V for 5 h, and finally 10,000 V for 6 h. Once IEF was completed, the strips were equilibrated in equilibration buffer (25 mM Tris–HCl, pH 8.8, 6 M urea, 20% glycerol, 2% SDS, and 130 mM DTT) for 15 min, followed by the same buffer containing 200 mM iodoacetamide instead of DTT for another 15 min. The second dimension was performed using 12% SDS-PAGE at 30 mA constant current per gel. The gels were stained using CBB R-250 (Merck, Germany) and scanned with a Bio-Rad GS-800 scanner. For each time point of treatment, duplicate or triplicate runs were made to ensure the accuracy of analyses. The maps were analyzed by PDQuest software Version 6.1 (Bio-Rad). The quantity of each spot in a gel was normalized as a percentage of the total quantity of all spots in that gel and evaluated in terms of OD. Only those spots that changed consistently and significantly (more than 1.5-fold) were selected for analysis with MS.

In-gel digestion

In-gel digestion of proteins was carried out using mass spectrometry grade Trypsin Gold (Promega, Madison, WI, USA) according to the manufacturer's instructions. Briefly, spots were cut out of the gel (1–2 mm diameter) using a razor blade, and destained twice with 100 mM NH_4HCO_3/50% acetonitrile (ACN) at 37°C for 45 min in each treatment. After dehydration and drying, the gels were preincubated in 10–20 (μl trypsin solution for 1 h. Then samples were added in adequate digestion buffer (40 mM NH_4HCO_3/10% ACN) to cover the gels and incubated overnight at 37°C. Tryptic digests were extracted using MiliQ water first, followed by extraction twice with 50% ACN/5% trifluoroacetic acid (TFA) for 1 h each time. The combined extracts were dried in a vacuum concentrator at room temperature. The samples were then subjected to mass spectrometric analysis.

MALDI-Q-TOF analysis and protein identification

Mass spectra were acquired using a Q-TOF mass spectrometer (Micromass, Manchester, UK) fitted with a MALDI source (Micromass). Tryptic digests were dissolved in 5 μl 70% ACN/0.1% TFA, and then 1 μl of the digests was mixed with 1 μl saturated alpha-cyano-4-hydroxy-cinnamic acid (CHCA) in 50% ACN/0.5% TFA and spotted onto a 96-well target plate. MS/MS was performed in a data-dependent mode in which the top ten most abundant ions for each MS scan were selected for MS/MS analysis. The MS/MS data were acquired and processed using MassLynx software (Micromass) and MASCOT was used to search the database. Database searches were carried out using the following parameters: Database, Swiss-Prot; taxonomy, *homo sapien*; enzyme, trypsin; and allowance of one missed cleavage. Carbamidomethylation was selected as a fixed modification and oxidation of methionine was allowed to be variable. The peptide and fragment mass tolerance were set at 1 and 0.2 Da, respectively. The data format was selected as Micromass PKL and the instrument was selected as MALDI-Q-TOF. Proteins with probability-based MOWSE scores exceeding their threshold ($P < 0.05$) were considered to be positively identified.

Semi-quantitative RT-PCR

Total RNAs were isolated using Trizol reagent (Invitrogen, Carlsbad, CA, USA) according to the manufacturer's instructions. First-strand cDNA was reversely transcribed from 1 μg total RNA in a final volume of 20 μl using RTase and random hexamers from ExScript ™ reagent kit (TAKARA, Dalian, China) according to manufacturer's instructions. Primers were designed mainly using Primer

Premier 5 software and a database search using NCBI blastn program was performed to ensure specificity. The primer sequences, expected annealing temperature and product length are listed in Table 1. PCR was performed with rTaq (TAKARA) in a gradient DNA thermal cycler (BioRad) according to a touchdown protocol as follows: 1 cycle of 95°C for 3 min; 10 cycles of 94°C for 45 s, annealing for 45 s (the annealing temperature was set to 5°C above the expected annealing temperature with a decrease by 1°C for every cycle), 72°C for 1 min; 25 additional cycles with the expected annealing temperature; a final extension at 72°C for 10 min and holding at 4°C. The amount of cDNA used for each PCR reaction was 20 ng in a 25 μl reaction volume. The PCR products (5 μl) were analyzed by electrophoresis through 2% agarose gels and visualized by SYBR Gold (Molecular Probes, Eugene, USA) staining.

Results

SAHA induced cell-growth inhibition and apoptosis in HepG2 cells

To determine the growth inhibitory activity of SAHA, MTT assay was performed on HepG2 cells. As shown in Fig. 1a, treatment with SAHA resulted in a marked decrease in cell survival, compared with untreated controls. Since the dose required for half-maximal inhibition of viability was 5 μM, this single concentration was subsequently utilized to treat HepG2 cancer cells in flow cytometry assay, TUNEL staining and 2-DE analysis.

In response to the treatment with 5 μM of SAHA for 48 h, HepG2 cells underwent morphological changes as shown in Fig. 1b. Elongated cells were readily seen with filamentous protrusions, cytoplasmic extensions and condensation of giant nucleus, indicating that the cells had undergone replicative senescence or apoptosis. SAHA-mediated HepG2 cell death was detected by flow cytometry (FACS) assay (Fig. 1c), in which a remarkable increase of SubG1 cell proportion was observed upon treatment with 5 μM SAHA, compared with the HepG2 control cells cultured in the presence of an equal amount of DMSO carrier ($P < 0.01$). As the sub-G1 value, measured by FACS, represents cells from both necrosis and apoptosis, a more sensitive assay (DeadEnd; fluorescence TUNEL system) was performed to allow detection of DNA strand breaks by labeling free 3-OH termini. Consistent with the FACS assay, there was a marked and significant increase of the apoptotic cells upon SAHA treatment ($P < 0.01$; Fig. 1e, f).

Comparison of the protein expression patterns between mock and SAHA-treated tumor cells

The protein expression profile of HepG2 cells before and after treatment with SAHA was examined at three time points (12, 24 and 48 h, respectively). Representative 2-DE maps of the three time intervals are shown in Fig. 2. By applying a threshold of 1.5-fold variation, a total of 55 spots were identified as differentially expressed after SAHA treatment. Out of the 55 spots, 34 proteins were identified by MS analysis. The identified spots were marked with arrows and numbers (Fig. 2), and the retrieved proteins corresponding to each numbered spots are listed in Table 2. The boxed areas in Fig. 2. indicated that these proteins also displayed significant expression changes at the earlier time points and their enlarged forms are shown in Fig. 4.

Table 1 Primers and PCR condition for each gene

Spot no.	Accession no.	Name	Primers	Annealing temperature (°C)	Product length (bp)
3	NM_002901	Reticulocalbin 1 precursor	Sense: 5′-gaccttcgaccagctcaccc-3′ Antisense: 5′-cggaattcgttaaactgctccc-3′	55	558
7	BC000260	Aldose reductase	Sense: 5′-ctggacctctaccttattcac-3′ Antisense: 5′-caccaccaagttcctctg-3′	53.3	468
8	BC000871	Annexin A3	Sense: 5′-tccgaaacatctggtgac-3′ Antisense: 5′-gccataatgcttcttgaactct-3′	50	453
15[a]	AB020027	Heat shock 27 kDa protein 1	Sense: 5′-ggcacgaggagcagagtcagc-3′ Antisense: ′-tggcgggggaggcacagc-3′	65	699
21	BC015100	Triosephosphate isomerase 1	Sense: 5′-gacatcatcaatgccaaaca-3′ Antisense: 5′-ggaacccaggagcaaatc-3′	53	308
24	X15132	Superoxide dismutase [Mn]	Sense: 5′-gacaaacctcagccctaa-3′ Antisense: 5′-cattctcccagttgattaca-3′	50	332
	BC083511	GAPDH	Sense: 5′-accacagtccatgccatcac-3′ Antisense: 5′-tccaccaccctgttgctgta-3′	55	452

[a] primers were published previously [22]

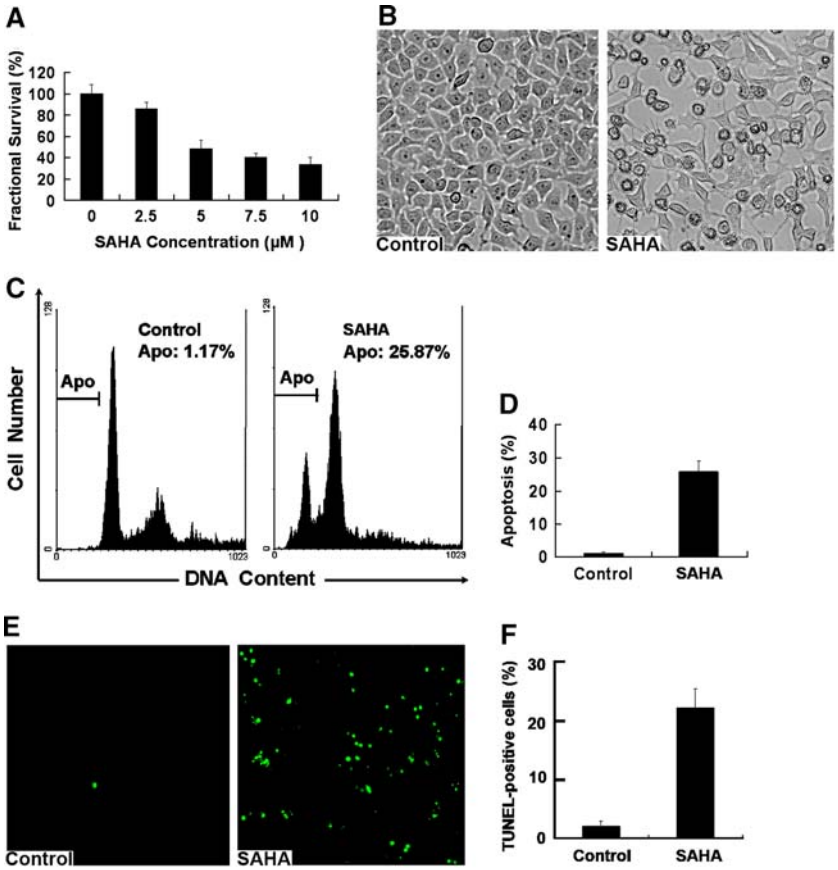

Fig. 1 Effects of SAHA on the proliferation and apoptosis of HepG2 cells. **a** Cells were treated with the indicated concentration of SAHA for 48 h, and cell proliferation was determined by MTT assay. After treatment, the cell viability (described as fractional survival) significantly decreased in a dose-dependent manner compared with the untreated control ($P < 0.05$). **b** Morphological change of HepG2 cells in response to 5 (μM SAHA treatment for 48 h (×200). **c**, **d** Flow cytometry analysis. After incubation with 5 μM SAHA for 48 h, the cells were stained with PI, and analyzed by flow cytometry. The results indicated that there was a significant increase in the percentage of apoptotic cells after treatment ($P < 0.01$). **e**, **f** TUNEL assays indicated a significant increase in the percentage of apoptotic cells after treatment (5 μM, 48 h, $P < 0.01$; ×100). For each sample, ≥500 cells were counted. All data are shown as mean values ± SD and are representative of three independent experiments performed in triplicate. *Apo* apoptotic percentage

To determine the generality of the changed proteins, a comparison of SAHA-induced protein alterations was performed between the HepG2 and Jurkat lymphoma cell lines. Patterns for the 34 differentially expressed proteins identified in HepG2 cells were also examined for the Jurkat cell lines, and of these, 18 proteins were unchanged, 12 proteins showed identical alteration trends, whilst 4 proteins showed opposite regulation trends following SAHA treatment (Figs. 3, 4; Table 2).

Protein identification

The 55 differentially expressed spots were subjected to MS/MS analysis, and database searching resulted in identification of 34 altered expression proteins (Fig. 2 and Table 2). A representative MALDI-TOF MS map of spot #8 is shown in Fig. 5a. Six intensity peaks (parent ions) in the map were subjected to MS/MS analysis. One of six MS/MS maps (m/z 1673.8963) obtained from fragmentation of the six parent ions is shown in Fig. 5b, and the query results showed this peptide sequence is LSPQAVNSIAK (Fig. 5c), which is a part of the sequence of protein Annexin A3. The query results with the MS/MS data are shown in Fig. 5c and d.

Semi-quantitative RT-PCR assay

To examine whether protein alterations observed by proteomic analysis correlate with the changes of those mRNAs at the transcription level, six proteins with significant expression changes (Figs. 2, 4) were chosen for further validation by semi-quantitative RT-PCR. As shown in Fig. 6, SAHA induced marked decreased transcripts in a time-dependent manner for the genes *RCN1* (Reticulocalbin 1 precursor), *ANXA3* (Annexin A3) and *HSP27* (Heat shock 27 kDa protein 1), while up-regulating the expression of *AR* (Aldose reductase), *TPI* (Triosephosphate isomerase 1) and *SOD2*

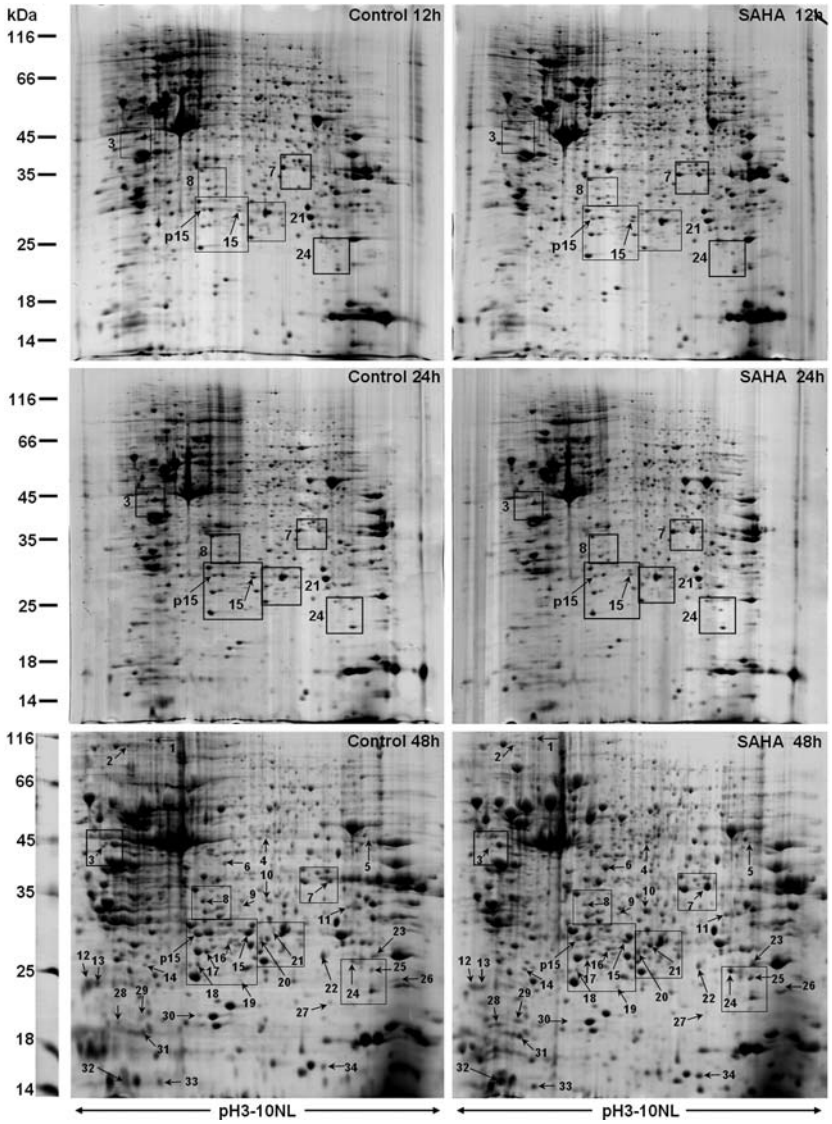

Fig. 2 Representative 2D gel images of HepG2 cells. Cells were treated with 5 μM SAHA for the indicated time points and with 0.05% DMSO as control. Total protein extracts were separated on pH 3–10 nonlinear IPG strips in the first dimension, followed by 12% SDS-PAGE in the second dimension and visualized by CBB staining. The *boxed areas* show proteins also with significant expression changes at the earlier time intervals and are shown in Fig. 4. in an *enlarged* form. A total of 34 differentially expressed spots were identified by MALDI-Q-TOF MS/MS (marked with *arrow* and *number*). Information on each numbered spot are reported in Table 2

(Manganese superoxide dismutase). Our data demonstrate that SAHA induced alterations in the expression of those genes at both transcription and translational levels (Figs. 2, 4).

Discussion

In the present study, human HepG2 cells were used as a model, and a 2DE-based proteomics approach was undertaken to annotate the altered proteins in HepG2 cells before and after treatment with SAHA. Consistent with previous studies [24], our data demonstrated that SAHA significantly induced the inhibition of cell growth and promoted apoptosis in HepG2 cancer cells. Proteomic analysis in this study revealed a total of 34 differentially expressed proteins, which functioned in diverse biological processes such as protein folding, metabolism, proteolysis, signal transduction, electron transport, as well as redox regulation. Among them, six proteins also displayed significant expression changes at earlier time points upon SAHA treatment, and these alterations were further confirmed by semi-quantitative RT-PCR analysis. Interestingly, observations from previous studies suggested that some protein expression alterations presented in this study were favored with the known antitumor activity of SAHA. The functional roles of the changed proteins associated with SAHA-mediated cell growth inhibition/cell death in liver cancer are briefly discussed below.

The proteins RCN1, ANXA3 and HSP27 are among those found to be down-regulated by SAHA. Firstly, RCN (the synonym of RCN1) was assumed to play a role in protein synthesis, modification and intracellular transport because of its localization in the lumen of the endoplasmic reticulum of a number of different types of cell [25, 26]. The RCN molecule was necessary for normal behavior of

Table 2 Identified proteins by MALDI-Q-TOF

Spot no.	Protein description	Function	Accession no.	Ther M_r/pI [a]	No. of pep.[b]	Score[c]	Expr level[d]	Jurkat cells
1	Heat shock 70 kDa protein 4	Molecular chaperon	P34932	95096/5.18	3	56	–	×
2	Endoplasmin precursor	Molecular chaperon	P14625	92696/4.76	3	46	–	×
3	Reticulocalbin 1 precursor	Signal transduction	Q15293	38866/4.86	2	75	–	×
4	Ornithine aminotransferase	Amino acid metabolism	P04181	48846/6.57	5	147	+	×
5	Ubiquinol-cytochrome-c reductase complex core protein 2	Electron transport	P22695	48584/8.74	5	183	+	×
6	Isocitrate dehydrogenase [NAD] subunit alpha	Metabolism	P50213	40022/6.47	6	132	+	I
7	Aldose reductase	Carbohydrate metabolism	P15121	36099/6.56	4	142	+	/
8	Annexin A3	Signal transduction	P12429	36393/5.63	6	249	–	×
9	Thiopurine S-methyltransferase	Nucleobase Metabolism	P51580	28618/5.84	2	75	+	×
10	Delta3,5-delta2,4-dienoyl-CoA isomerase	Lipid metabolism	Q13011	36136/8.16	4	165	+	×
11	Electron transfer flavoprotein subunit alpha	Electron transport	P13804	35400/8.62	2	104	+	I
12	Prostaglandin E synthase 3	Telomere maintenance and biosynthesis	Q15185	18971/4.35	2	102	–	I
13[e]	Prostaglandin E synthase 3	Telomere maintenance and biosynthesis	Q15185	18971/4.35	1	66	–	×
13[e]	Interleukin-18 precursor	Signal transduction	Q14116	22597/4.54	3	52	–	×
14	NADH-ubiquinone oxidoreductase 23 kDa subunit	Electron transport	O00217	24203/6.00	3	108	+	×
15	Heat-shock protein beta-1	Molecular chaperon	P04792	22826/5.98	2	96	–	×
p15[f]	Heat-shock protein beta-1	Molecular chaperon	P04792	22826/5.98	3	122	–	×
16	Ribosyldihydronicotinamide dehydrogenase	Electron transport	P16083	26033/5.89	4	146	+	×
17[e]	Proteasome subunit beta type 4 precursor	Proteolysis	P28070	29230/5.72	3	106	–	×
17[e]	Glutathione S-transferase P	Metabolism	P09211	23438/5.44	2	75	–	×
18	Ras-related protein Rab-11B	Signal transduction	Q15907	24456/5.65	4	110	–	×
19	Phosphomevalonate kinase	Lipid metabolism	Q15126	22021/5.57	2	114	+	×
20[e]	Thioredoxin-dependent peroxide reductase	Redox regulation	P30048	28017/7.67	2	83	+	×
20[e]	Transforming protein RhoA precursor	Signal transduction	P61586	22096/5.83	1	31	+	×
21	Triosephosphate isomerase 1	Metabolism	P60174	26807/6.51	3	139	+	×
22	Proteasome subunit beta type 2	Proteolysis	P49721	22993/6.51	3	117	–	I
23	Peroxiredoxin-1	Redox regulation	Q06830	22324/8.27	3	102	+	I
24	Superoxide dismutase [Mn]	Redox regulation	P04179	24878/8.35	3	89	+	I
25	Flavin reductase	Nucleotide-sugar metabolism	P30043	21974/7.31	2	46	+	/
26	Cellular nucleic acid-binding protein	Signal transduction	P62633	20704/8.00	1	58	–	×
27	Ufm1-conjugating enzyme 1	Proteolysis	Q9Y3C8	19626/6.96	2	34	–	I
28	MIR-interacting saposin-like protein precursor	Signal transduction	Q9Y2B0	20981/4.81	4	245	+	I
29	Hippocalcin-like protein 1	Signal transduction	P37235	22282/5.21	5	103	+	I
30	1,2-dihydroxy-3-keto-5-methylthiopentene dioxygenase	Amino acid Metabolism	Q9BV57	21542/5.43	4	46	–	I
31	Eukaryotic translation initiation factor 5A-1	Transcription	P63241	16918/5.08	3	171	+	I
32	Thioredoxin	Redox regulation	P10599	11884/4.82	3	59	+	/

Table 2 continued

Spot no.	Protein description	Function	Accession no.	Ther M_r/pI [a]	No. of pep.[b]	Score[c]	Expr level[d]	Jurkat cells
33	Thioredoxin-like protein 5	Redox regulation	Q9BRA2	14217/5.40	2	85	+	/
34	Cytochrome c oxidase polypeptide Vb	Electron transport	P10606	13915/9.07	2	53	+	|

(×, no corresponding protein spots were found in Jurkat cells; |, changed in a consistent manner in Jurkat cells compared with HepG2 cells; /, changed in a reverse manner in Jurkat cells compared with HepG2 cells

[a] Theoretical molecular weight (kDa) and pI from the ExPASy database

[b] The number of unique peptides identified by MS/MS sequencing

[c] Probability-based MOWSE scores

[d] Expression level in SAHA-treated HepG2 cells at the time point of 48 h compared with control (+, increase; −, decrease)

[e] Two proteins were identified from a single spot

[f] Phosphorylated form of spot #15 [22, 23]

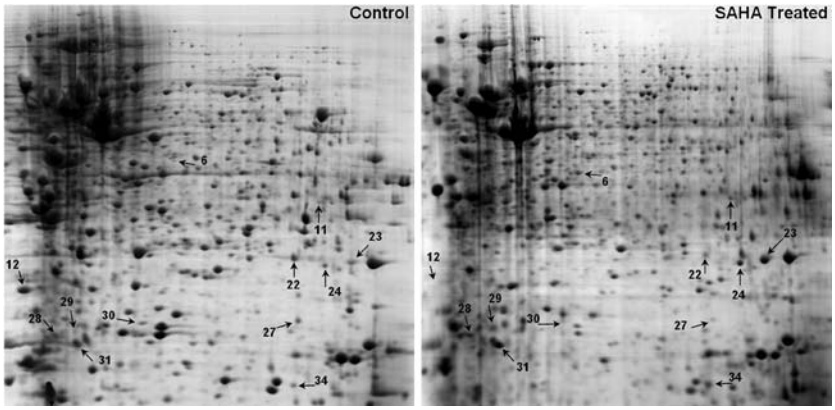

Fig. 3 Representative 2D gel images of Jurkat cells. Twelve protein spots (marked with *arrow* and *number*) display consistent alterations compared with the changed proteins in HepG2 cells upon SAHA treatment. Information on the changed patterns of these spots are listed in Table 2

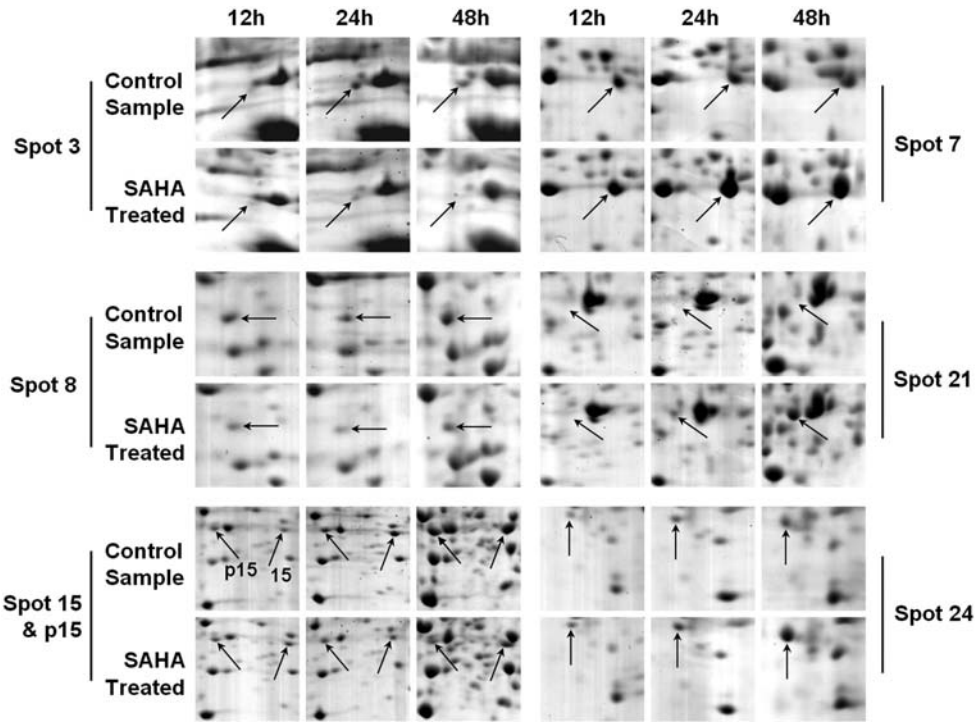

Fig. 4 Enlargement of selected regions in Fig. 2. showing the differentially expressed protein spots. Protein p15 is the phosphorylated form of protein #15. The spots (#3, #8, #15, p15) in the *left panels* and spots (#7, #21, #24) in the *right panels* correspond to down- or up-regulated spots, respectively (note that the amount of protein loading in the 48 h treated interval are three times the amount used in the 12 and 24 h intervals). Differential expression of spots #3, #15, p15 and #21 in the 12 h treated interval are not observed. Information on these spots are reported in Table 2

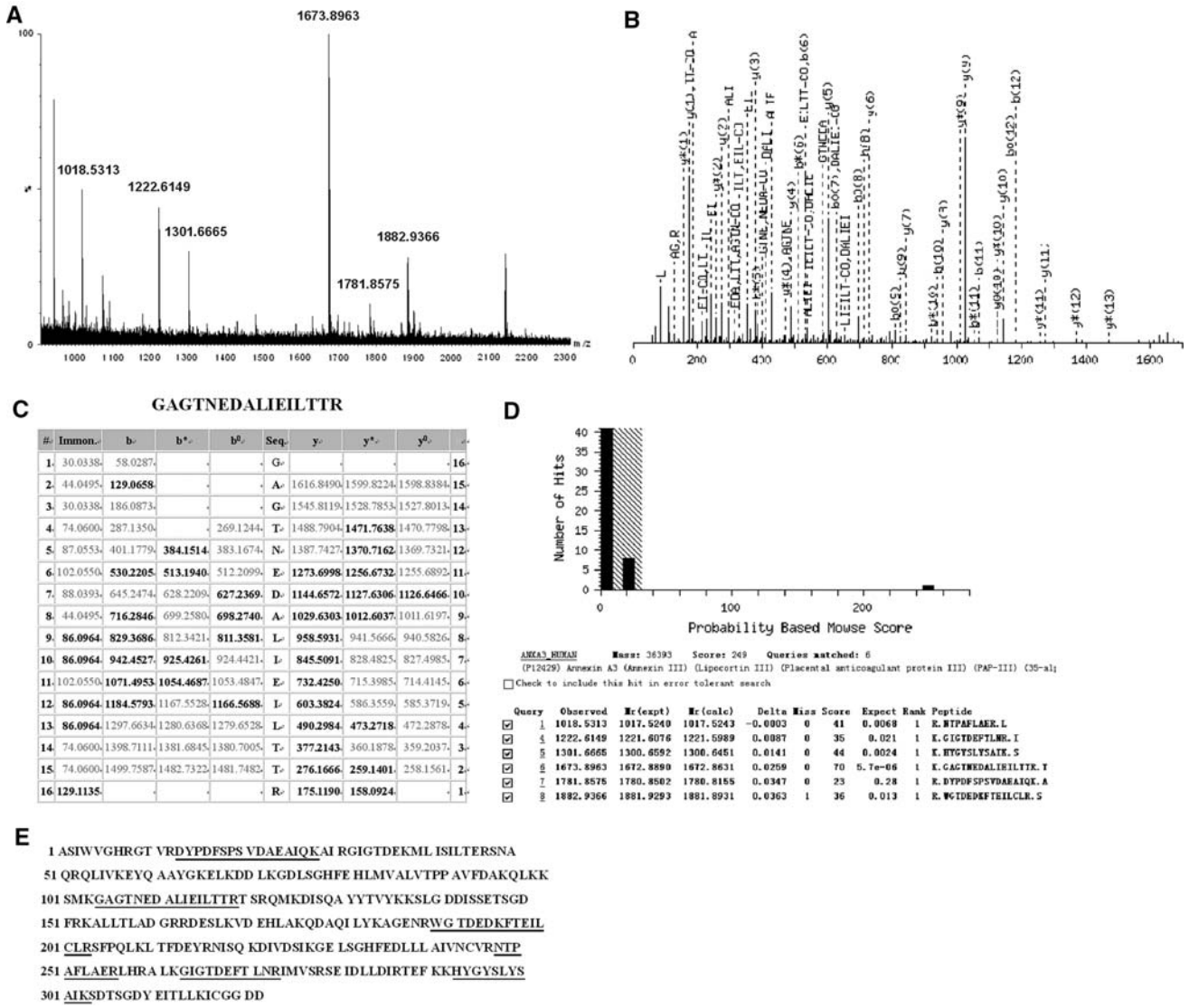

#.	Immon.	b.	b*.	b0.	Seq.	y.	y*.	y0.	
1.	30.0338.	58.0287.			G.				16.
2.	44.0495.	**129.0658.**			A.	1616.8490.	1599.8224.	1598.8384.	15.
3.	30.0338.	186.0873.			G.	1545.8119.	1528.7853.	1527.8013.	14.
4.	74.0600.	287.1350.		269.1244.	T.	1488.7904.	**1471.7638.**	1470.7798.	13.
5.	87.0553.	401.1779.	**384.1514.**	383.1674.	N.	1387.7427.	**1370.7162.**	1369.7321.	12.
6.	102.0550.	**530.2205.**	**513.1940.**	512.2099.	E.	**1273.6998.**	**1256.6732.**	1255.6892.	11.
7.	88.0393.	645.2474.	628.2209.	**627.2369.**	D.	**1144.6572.**	**1127.6306.**	**1126.6466.**	10.
8.	44.0495.	**716.2846.**	699.2580.	**698.2740.**	A.	**1029.6303.**	**1012.6037.**	1011.6197.	9.
9.	**86.0964.**	**829.3686.**	812.3421.	**811.3581.**	L.	**958.5931.**	941.5666.	940.5826.	8.
10.	**86.0964.**	**942.4527.**	**925.4261.**	924.4421.	I.	**845.5091.**	828.4825.	827.4985.	7.
11.	102.0550.	**1071.4953.**	**1054.4687.**	1053.4847.	E.	**732.4250.**	715.3985.	714.4145.	6.
12.	**86.0964.**	**1184.5793.**	1167.5528.	**1166.5688.**	I.	**603.3824.**	586.3559.	585.3719.	5.
13.	**86.0964.**	1297.6634.	1280.6368.	1279.6528.	L.	**490.2984.**	**473.2718.**	472.2878.	4.
14.	74.0600.	1398.7111.	1381.6845.	1380.7005.	T.	**377.2143.**	360.1878.	359.2037.	3.
15.	74.0600.	1499.7587.	1482.7322.	1481.7482.	T.	**276.1666.**	**259.1401.**	258.1561.	2.
16.	**129.1135.**				R.	**175.1190.**	**158.0924.**		1.

Fig. 5 Identification of protein spot #8. **a** Mass spectrogram of tryptic peptides from spot #8. Six peptides with *m/z* values were subjected to MS/MS analysis. **b** An example of an MS/MS spectrum of parent ion 1673.8963. **c**, **d** Output of the database searching by the MASCOT program using MS/MS data resulted in the identification of Annexin A3. **e** Protein sequence of Annexin A3 is shown. The matched peptides are *underlined*

cells because homozygous deletion in mice of RCN could contribute to the lethality [27]. Although the detailed physiological functions of RCN remain unknown, Yu et al. [28] reported that RCN was over-expressed in hepatoma cancer cells compared to normal liver cells. Further, Liu et al. [29] found RCN expressed in highly invasive breast cancer cell lines, but not in poorly invasive cell lines. These studies suggested that over-expression of RCN was implicated with certain tumor development. Secondly, ANXA3 is a member of the ANX family. Every ANX has a conserved core domain consisting of 4 or 8 annexin repeats, through which ANX binds to phospholipids in a Ca^{2+}-dependent manner [30]. Of the ANX family members, ANXA3 is one of the least known members in terms of function [31]. Niimi et al. [32] recently reported that inhibition of ANXA3 expression by RNA interference resulted in a significant inhibition of parenchymal rat hepatocyte growth, indicating that ANXA3 acted as a positive regulator on hepatocyte growth in cultured hepatocytes. Thirdly, over-expression of HSPs was associated with a wide range of human cancers with a poor prognosis and resistance to therapy. The HSP family members play overlapping, essential roles in cancer cell growth, both by promoting autonomous cell proliferation and by inhibiting death pathways. The HSPs have become targets for rational anticancer drug design [33, 34]. HSP27 belongs to the HSP family and has been shown to prevent apoptosis by suppressing the activation of procaspase 9 [35] and regulating Akt activation [36]

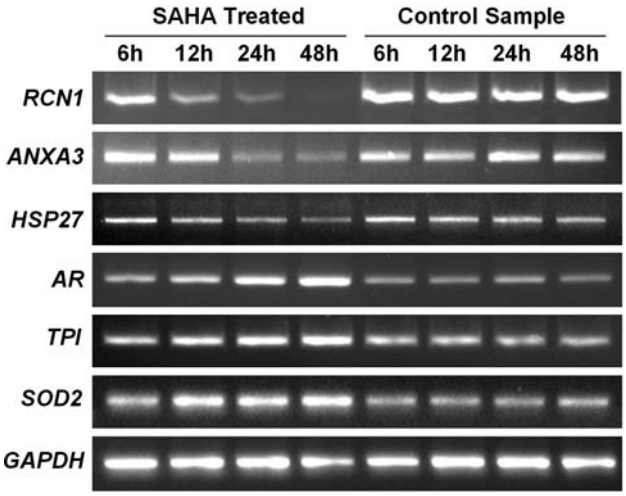

Fig. 6 Semi-quantitative RT-PCR confirmation of the six genes corresponding to the six spots in 2 and 4. HepG2 cells were exposed to 5 μM SAHA for the indicated time durations with 0.05% DMSO as control. The images are the representative results of at least three independent experiments. As shown, SAHA treatment inhibits the mRNA expression of *RCN1*, *ANXA3* and *HSP27* corresponding to protein spots #3, #8, #15 and p15 in Figs. 2 and 4, while stimulating *AR*, *TPI*, and *SOD2* corresponding to spot #7, #21 and #24, respectively. *GAPDH* was used as a loading control

as well as inhibiting the activation of NF-kappa B [37]. HSP90 inhibitors are showing much promise in clinical trials and among them 17-AAG has reached phase II clinical trials [38]. Together, studies have shown that over-expression of RCN1, ANXA3 and HSP27 was routinely associated with a wide range of tumor origins including liver cancer. Down-regulation of these proteins may play a role in SAHA-mediated growth inhibition of HepG2 cancer cells, as well as induction of apoptosis. Further studies will be conducted to elucidate the possible crosstalk between the reduced expression of RCN1, ANXA3, and HSP27 and SAHA-mediated inhibition of liver cancer cell growth and induction of apoptosis.

In contrast, our studies demonstrated that SOD2, AR, and TPI were markedly up-regulated in SAHA-treated HepG2 cells. Firstly, SOD2 was an important antioxidant enzyme that functioned to attenuate oxidative free radicals in the mitochondria by catalyzing the formation of hydrogen peroxide from superoxide radicals. SOD2 is a tumor necrosis factor (TNF)-inducible gene product [39] and has been suggested to be a tumor suppressor gene in a variety of cancer cells such as melanoma [40], pancreatic cancer [41], prostate cancer [42] and breast cancer cells [43]. Recently Hodge et al. [44] reported that enforced expression of SOD2 could enhance dexamethasone-induced apoptosis in human multiple myeloma cells. Secondly, AR is a member of the aldo-keto reductase family, and has been shown to play an important role in the development of complications in diabetes [45]. However, recently accumulated evidence suggested that AR was involved in regulating apoptosis. In pancreatic beta-cells, AR activation induced apoptosis by causing an imbalance in redox status [46]. Galvez et al. [47] found that cell death induced by hyperosmolarity required induction of AR as well as a decrease in intracellular glutathione levels. Ramana et al. [48] suggested that AR was a critical regulator of TNF-α-induced apoptotic signaling in endothelial cells. AR was also found to play a key role in galactose-induced apoptosis of lens epithelial cell [49] and in glucose-induced apoptosis of cultured retinal pericytes [50]. Thirdly, studies have revealed that glycolytic enzyme TPI can be induced as a stress protein by hypoxia [51], chemical carcinogen promoters [52] and high iron concentration [53]. Together, considering either the tumor-suppressing activity of SOD2 or the apoptosis-inducing activity of AR, up-regulation of these two proteins should play a role in SAHA-mediated growth retardation of HepG2 cancer cells and/or induction of cell death. Although it remained unclear as to the functional importance of up-regulation of TPI proteins, previous studies demonstrated that it was a common outcome under the conditions of cellular stress. Further studies will be required to address if up-regulation of cellular stress protein TPI plays a role in SAHA-mediated suppression of HepG2 cell growth.

In this study, a total of 55 altered proteins were visualized by 2-DE and Coomassie Brilliant Blue (CBB) staining. Many cellular regulatory proteins that are known to be influenced by HDAC inhibitors, for example, p21, p53, E2F-1, cyclin E, cyclin D1, etc. [7, 9, 54–56], were not revealed and this was possibly due to their low abundance. More comprehensive analyses will be performed to identify the altered low-abundance cellular factors by using large-size gel slabs, depletion high-abundance proteins, enrichment of the samples by prefractionation and by using silver staining coupled with LC-MS/MS analysis [57, 58].

SAHA has been reported to induce cell growth inhibition and/or apoptosis in a variety of tumor cells. But the IC_{50} values vary widely for different tumor types and different cell lines. For example, the IC_{50} values were 0.65–5 μM for CTCL and other lymphomas [21, 59], 2–8 μM for gastric cancer [60], 5–20 μM for ovarian carcinoma [61], etc. In the current study, we observed that the IC_{50} value for HepG2 was 5 μM, suggesting a moderate sensitivity. Cancer cells are defective in some of their signaling pathways due to genetic/epigenetic alterations of certain genes; this could explain why some cells are sensitive to SAHA whereas others are very resistant. SAHA-induced cellular protein alterations would likely be cell type/cancer cell specific, despite the fact that SAHA could mediate some common protein changes in most cancer types including p21, E2F-1, cyclin E, cyclin D1, etc. In the comparison of protein changes between HepG2 and Jurkat cell lines in

response to SAHA treatment, we found that only 12 out of the 34 identified proteins displayed consistent expression alterations (Fig. 3; Table 2). Further studies will be performed regarding the generality of the protein alterations in different cell types upon SAHA treatment.

In conclusion, this study demonstrated that SAHA induced significant growth inhibition and apoptosis in human hepatocellular carcinoma cell line HepG2. Using a proteomics strategy, we identified 34 differentially expressed proteins. Among them, six proteins also displayed significant expression changes at earlier time points upon SAHA treatment. And of the six proteins, SAHA mediated down-regulation of the oncoproteins, RCN1, ANXA3 and HSP27, and up-regulation of tumor suppressor and apoptosis-related proteins, SOD2 and AR. These effects are thought to be associated with the antitumor activity of SAHA in HepG2 cells.

Acknowledgments This work was supported by grants from the National 973 Basic Research Program of China (2004CB518807, 2006CB504303 and 2006CB504302) and the Sichuan Applied Basic Research (07JY029-052).

References

1. Richon VM, Emiliani S, Verdin E, Webb Y, Breslow R, Rifkind RA et al (1998) A class of hybrid polar inducers of transformed cell differentiation inhibits histone deacetylases. Proc Natl Acad Sci USA 95:3003–3007
2. Narlikar GJ, Fan HY, Kingston RE (2002) Cooperation between complexes that regulate chromatin structure and transcription. Cell 108:475–487
3. Butler LM, Agus DB, Scher HI, Higgins B, Rose A, Cordon-Cardo C et al (2000) Suberoylanilide hydroxamic acid, an inhibitor of histone deacetylase, suppresses the growth of prostate cancer cells in vitro and in vivo. Cancer Res 60:5165–5170
4. Cao ZA, Bass KE, Balasubramanian S, Liu L, Schultz B, Verner E et al (2006) CRA-026440: a potent, broad-spectrum, hydroxamic histone deacetylase inhibitor with antiproliferative and antiangiogenic activity in vitro and in vivo. Mol Cancer Ther 5:1693–1701
5. Finnin MS, Donigian JR, Cohen A, Richon VM, Rifkind RA, Marks PA et al (1999) Structures of a histone deacetylase homologue bound to the TSA and SAHA inhibitors. Nature 401:188–193
6. Marks P, Rifkind RA, Richon VM, Breslow R, Miller T, Kelly WK (2001) Histone deacetylases and cancer: causes and therapies. Nat Rev Cancer 1:194–202
7. Richon VM, Sandhoff TW, Rifkind RA, Marks PA (2000) Histone deacetylase inhibitor selectively induces p21WAF1 expression and gene-associated histone acetylation. Proc Natl Acad Sci USA 97:10014–10019
8. Ruefli AA, Ausserlechner MJ, Bernhard D, Sutton VR, Tainton KM, Kofler R et al (2001) The histone deacetylase inhibitor and chemotherapeutic agent suberoylanilide hydroxamic acid (SAHA) induces a cell-death pathway characterized by cleavage of Bid and production of reactive oxygen species. Proc Natl Acad Sci USA 98:10833–10838
9. Henderson C, Mizzau M, Paroni G, Maestro R, Schneider C, Brancolini C et al (2003) Role of caspases, Bid, and p53 in the apoptotic response triggered by histone deacetylase inhibitors trichostatin: a (TSA) and suberoylanilide hydroxamic acid (SAHA). J Biol Chem 278:12579–12589
10. Takada Y, Gillenwater A, Ichikawa H, Aggarwal BB (2006) Suberoylanilide hydroxamic acid potentiates apoptosis, inhibits invasion, and abolishes osteoclastogenesis by suppressing nuclear factor-kappaB activation. J Biol Chem 281:5612–5622
11. Xu W, Ngo L, Perez G, Dokmanovic M, Marks PA (2006) Intrinsic apoptotic and thioredoxin pathways in human prostate cancer cell response to histone deacetylase inhibitor. Proc Natl Acad Sci USA 103:15540–15545
12. El-Serag HB, Davila JA, Petersen NJ, McGlynn KA (2003) The continuing increase in the incidence of hepatocellular carcinoma in the United States: an update. Ann Intern Med 139:817–823
13. Wilson JF (2005) Liver cancer on the rise. Ann Intern Med 142:1029–1032
14. Cormier JN, Thomas KT, Chari RS, Pinson CW (2006) Management of hepatocellular carcinoma. J Gastrointest Surg 10:761–780
15. Herold C, Ganslmayer M, Ocker M, Hermann M, Geerts A, Hahn EG et al (2002) The histone-deacetylase inhibitor Trichostatin A blocks proliferation and triggers apoptotic programs in hepatoma cells. J Hepatol 36:233–240
16. Yamashita Y, Shimada M, Harimoto N, Rikimaru T, Shirabe K, Tanaka S et al (2003) Histone deacetylase inhibitor trichostatin A induces cell-cycle arrest/apoptosis and hepatocyte differentiation in human hepatoma cells. Int J Cancer 103:572–576
17. Armeanu S, Pathil A, Venturelli S, Mascagni P, Weiss Thomas S, Gottlicher M et al (2005) Apoptosis on hepatoma cells, but not on primary hepatocytes by histone deacetylase inhibitors valproate and ITF2357. J Hepatol 42:210–217
18. Jain KK (2000) Applications of proteomics in oncology. Pharmacogenomics 1:385–393
19. Kabuyama Y, Resing KA, Ahn NG (2004) Applying proteomics to signaling networks. Curr Opin Genet Dev 14:492–498
20. Holly MK, Dear JW, Hu X, Schechter AN, Gladwin MT, Hewitt SM et al (2006) Biomarker and drug-target discovery using proteomics in a new rat model of sepsis-induced acute renal failure. Kidney Int 70:496–506
21. Sakajiri S, Kumagai T, Kawamata N, Saitoh T, Said JW, Koeffler HP (2005) Histone deacetylase inhibitors profoundly decrease proliferation of human lymphoid cancer cell lines. Exp Hematol 33:53–61
22. Song H, Ethier SP, Dziubinski ML, Lin J (2004) Stat3 modulates heat shock 27 kDa protein expression in breast epithelial cells. Biochem Biophys Res Commun 314:143–150
23. Neo JCH, Rose P, Ong CN, Chung MCM (2005) Beta-phenylethyl isothiocyanate mediated apoptosis: a proteomic investigation of early apoptotic protein changes. Proteomics 5:1075–1082
24. Gray SG, Qian CN, Furge K, Guo X, Teh BT (2004) Microarray profiling of the effects of histone deacetylase inhibitors on gene expression in cancer cell lines. Int J Oncol 24:773–795
25. Ozawa M, Muramatsu T (1993) Reticulocalbin, a novel endoplasmic reticulum resident $Ca(2^+)$-binding protein with multiple EF-hand motifs and a carboxyl-terminal HDEL sequence. J Biol Chem 268:699–705
26. Tachikui H, Navet AF, Ozawa M (1997) Identification of the $Ca(2^+)$-binding domains in reticulocalbin, an endoplasmic reticulum resident $Ca(2^+)$-binding protein with multiple EF-hand motifs. J Biochem (Tokyo) 121:145–149
27. Kent J, Lee M, Schedl A, Boyle S, Fantes J, Powell M et al (1997) The reticulocalbin gene maps to the WAGR region in human and to the small eye Harwell deletion in mouse. Genomics 42:260–267
28. Yu LR, Zeng R, Shao XX, Wang N, Xu YH, Xia QC (2000) Identification of differentially expressed proteins between human hepatoma and normal liver cell lines by two-dimensional electrophoresis and liquid chromatography-ion trap mass spectrometry. Electrophoresis 21:3058–3068

29. Liu Z, Brattain MG, Appert H (1997) Differential display of reticulocalbin in the highly invasive cell line, MDA-MB-435, versus the poorly invasive cell line, MCF-7. Biochem Biophys Res Commun 231:283–289
30. Gerke V, Moss SE (2002) Annexins: from structure to function. Physiol Rev 82:331–371
31. Hsiang CH, Tunoda T, Whang YE, Tyson DR, Ornstein DK (2006) The impact of altered annexin I protein levels on apoptosis and signal transduction pathways in prostate cancer cells. Prostate 66:1413–1424
32. Niimi S, Harashima M, Gamou M, Hyuga M, Seki T, Ariga T et al (2005) Expression of annexin A3 in primary cultured parenchymal rat hepatocytes and inhibition of DNA synthesis by suppression of annexin A3 expression using RNA interference. Biol Pharm Bull 28:424–428
33. Ciocca DR, Calderwood SK (2005) Heat shock proteins in cancer: diagnostic, prognostic, predictive, and treatment implications. Cell Stress Chaperones 10:86–103
34. Calderwood SK, Khaleque MA, Sawyer DB, Ciocca DR (2006) Heat shock proteins in cancer: chaperones of tumorigenesis. Trends Biochem Sci 31:164–172
35. Garrido C, Bruey JM, Fromentin A, Hammann A, Arrigo AP, Solary E (1999) HSP27 inhibits cytochrome c-dependent activation of procaspase-9. FASEB J 13:2061–2070
36. Rane MJ, Pan Y, Singh S, Powell DW, Wu R, Cummins T et al (2003) Heat shock protein 27 controls apoptosis by regulating Akt activation. J Biol Chem 278:27828–27835
37. Kammanadiminti SJ, Chadee K (2006) Suppression of NF-kappaB activation by *Entamoeba histolytica* in intestinal epithelial cells is mediated by heat shock protein 27. J Biol Chem 281:26112–26120
38. Pacey S, Banerji U, Judson I, Workman P (2006) Hsp90 inhibitors in the clinic. Handb Exp Pharmacol 172:331–358
39. Guo Z, Boekhoudt GH, Boss JM (2003) Role of the intronic enhancer in tumor necrosis factor-mediated induction of manganous superoxide dismutase. J Biol Chem 278:23570–23578
40. Church SL, Grant JW, Ridnour LA, Oberley LW, Swanson PE, Meltzer PS et al (1993) Increased manganese superoxide dismutase expression suppresses the malignant phenotype of human melanoma cells. Proc Natl Acad Sci USA 90:3113–3117
41. Weydert C, Roling B, Liu J, Hinkhouse MM, Ritchie JM, Oberley LW et al (2003) Suppression of the malignant phenotype in human pancreatic cancer cells by the overexpression of manganese superoxide dismutase. Mol Cancer Ther 2:361–369
42. Venkataraman S, Jiang X, Weydert C, Zhang Y, Zhang HJ, Goswami PC et al (2005) Manganese superoxide dismutase overexpression inhibits the growth of androgen-independent prostate cancer cells. Oncogene 24:77–89
43. Weydert CJ, Waugh TA, Ritchie JM, Iyer KS, Smith JL, Li L et al (2006) Overexpression of manganese or copper-zinc superoxide dismutase inhibits breast cancer growth. Free Radic Biol Med 41:226–237
44. Hodge DR, Xiao W, Peng B, Cherry JC, Munroe DJ, Farrar WL (2005) Enforced expression of superoxide dismutase 2/manganese superoxide dismutase disrupts autocrine interleukin-6 stimulation in human multiple myeloma cells and enhances dexamethasone-induced apoptosis. Cancer Res 65:6255–6263
45. Yabe-Nishimura C (1998) Aldose reductase in glucose toxicity: a potential target for the prevention of diabetic complications. Pharmacol Rev 50:21–33
46. Hamaoka R, Fujii J, Miyagawa J, Takahashi M, Kishimoto M, Moriwaki M et al (1999) Overexpression of the aldose reductase gene induces apoptosis in pancreatic beta-cells by causing a redox imbalance. J Biochem (Tokyo) 126:41–47
47. Galvez AS, Ulloa JA, Chiong M, Criollo A, Eisner V, Barros LF et al (2003) Aldose reductase induced by hyperosmotic stress mediates cardiomyocyte apoptosis: differential effects of sorbitol and mannitol. J Biol Chem 278:38484–38494
48. Ramana KV, Bhatnagar A, Srivastava SK (2004) Inhibition of aldose reductase attenuates TNF-alpha-induced expression of adhesion molecules in endothelial cells. FASEB J 18:1209–1218
49. Murata M, Ohta N, Sakurai S, Alam S, Tsai J, Kador PF et al (2001) The role of aldose reductase in sugar cataract formation: aldose reductase plays a key role in lens epithelial cell death (apoptosis). Chem Biol Interact 130–132:617–625
50. Miwa K, Nakamura J, Hamada Y, Naruse K, Nakashima E, Kato K et al (2003) The role of polyol pathway in glucose-induced apoptosis of cultured retinal pericytes. Diabetes Res Clin Pract 60:1–9
51. Gess B, Hofbauer KH, Deutzmann R, Kurtz A (2004) Hypoxia upregulates triosephosphate isomerase expression via an HIF-dependent pathway. Pflugers Arch 448:175–180
52. Jiang PZ, Gan M, Huang H, Shen XM, Wang S, Yao KT (2005) Proteomics-based identification of proteins with altered expression induced by 12-O-tetradecanoylphorbol 13-acetate in nasopharyngeal carcinoma CNE2 cells. Acta Biochim Biophys Sin (Shanghai) 37:97–106
53. Lieu HY, Song HS, Yang SN, Kim JH, Kim HJ, Park YD et al (2006) Identification of proteins affected by iron in *Saccharomyces cerevisiae* using proteome analysis. J Microbiol Biotechnol 16:946–951
54. Richon VM (2006) Cancer biology: mechanism of antitumour action of vorinostat (suberoylanilide hydroxamic acid), a novel histone deacetylase inhibitor.95(Suppl 1):S2–S6
55. Bolden JE, Peart MJ, Johnstone RW (2006) Anticancer activities of histone deacetylase inhibitors. Nat Rev Drug Discov 5:769–784
56. Minucci S, Pelicci PG (2006) Histone deacetylase inhibitors and the promise of epigenetic (and more) treatments for cancer. Nat Rev Cancer 6:38–51
57. Lescuyer P, Hochstrasser DF, Sanchez JC (2004) Comprehensive proteome analysis by chromatographic protein prefractionation. Electrophoresis 25:1125–1135
58. Corthals GL, Wasinger VC, Hochstrasser DF, Sanchez JC (2000) The dynamic range of protein expression: a challenge for proteomic research. Electrophoresis 21:1104–1115
59. Zhang CL, Richon V, Ni X, Talpur R, Duvic M (2005) Selective induction of apoptosis by histone deacetylase inhibitor SAHA in cutaneous T-cell lymphoma cells: relevance to mechanism of therapeutic action. J Invest Dermatol 125:1045–1052
60. Huang C, Ida H, Ito K, Zhang H, Ito Y (2007) Contribution of reactivated RUNX3 to inhibition of gastric cancer cell growth following suberoylanilide hydroxamic acid (vorinostat) treatment. Biochem Pharmacol 73:990–1000
61. Sonnemann J, Gange J, Pilz S, Stotzer C, Ohlinger R, Belau A et al (2006) Comparative evaluation of the treatment efficacy of suberoylanilide hydroxamic acid (SAHA) and paclitaxel in ovarian cancer cell lines and primary ovarian cancer cells from patients. BMC Cancer 6:183